



PCCP

Resonance-assisted intramolecular triel bonds

Journal:	<i>Physical Chemistry Chemical Physics</i>
Manuscript ID	CP-ART-03-2022-001244.R1
Article Type:	Paper
Date Submitted by the Author:	26-May-2022
Complete List of Authors:	Liu, Na; Yantai University Li, Qingzhong; Yantai University Scheiner, Steve; Utah State University, Department of Chemistry and Biochemistry Xie, Xiaoying; Yantai University,

SCHOLARONE™
Manuscripts

Resonance-Assisted Intramolecular Triel Bonds

Na Liu,^a Qingzhong Li,^{*,a} Steve Scheiner,^{*,b} Xiaoying Xie^{*,a}

^a The Laboratory of Theoretical and Computational Chemistry, School of Chemistry and Chemical Engineering, Yantai University, Yantai 264005, P. R. China.

^b Department of Chemistry and Biochemistry, Utah State University, Logan, UT 84322-0300, USA

Corresponding authors: Qingzhong Li, Steve Scheiner, and Xiaoying Xie

E-mail: lqz@ytu.edu.cn, steve.scheiner@usu.edu, and 202007000015@ytu.edu.cn

Abstract

The possibility that the intramolecular $\text{Tr}\cdots\text{S}$ triel bond is strengthened by resonance is examined by quantum chemical calculations within the planar five-membered ring of $\text{TrH}_2\text{-CR=CR-CR=S}$ ($\text{Tr} = \text{Al, Ga, In}$; $\text{R} = \text{NO}_2, \text{CH}_3$). This internal bond is found to be rather short (2.4-2.7 Å) with a large bond energy between 12 and 21 kcal/mol. The pattern of bond length alternation and atomic charges within the ring is consistent with resonance involving the conjugated double bonds. This resonance enhances the triel bond strength by some 25%. The electron-withdrawing NO_2 group weakens the bond, but it is strengthened by the electron-donating CH_3 substituent. NICS analysis suggests the presence of a certain degree of aromaticity within the ring.

Keywords: Conjugation; Substituent effects; QTAIM; NICS

1. Introduction

Non-covalent interactions play a crucial role in chemistry, biology, and materials science. They can stabilize the structure of a molecule,¹ lower the activation energy of a chemical reaction,² construct supramolecular materials,³ and modulate the properties of crystal materials.⁴ These applications are so numerous due to their diversity, which encompass the hydrogen bond⁵, alkaline-earth bond,⁶ regium bond,⁷ spodium bond,⁸ pnictogen bond,⁹ chalcogen bond,¹⁰ halogen bond,¹¹ aerogen bond,¹² tetrel bond,¹³ and triel bond.¹⁴ The incorporation of the way in which the molecular electrostatic potential (MEP) surrounding each subunit,¹⁵ has deepened our understanding of noncovalent interactions which involve almost all main group elements and even subgroup elements.

One of this class, the triel bond, was proposed¹⁴ to describe the noncovalent interaction between a Group 3 atom and an electron-rich nucleophile. The empty p orbital on a trivalent triel atom (e.g. trihydrides and trihalides) leads to a π -hole, a region with positive MEPS, above the molecular plane, which contributes to the high directionality of this bond. The recent literature has expanded with experimental and theoretical studies of the triel bond and particularly its relation to chemical reactivity.¹⁶⁻¹⁸

The H-bond can be considered in some ways as the parent of many of these noncovalent bonds. These bonds are important in establishing the structure and function of important molecules such as proteins.^{19,20} Internal H-bonds which link two segments of the same molecule are also involved in supramolecular recognition.^{21,22} Inspired by internal interactions of this type, research has dealt with other intramolecular contacts, as for example pnictogen,²³ tetrel,²⁴ or chalcogen bonds.²⁵ However, research involving intramolecular triel bonds remains scant.

The manner in which substituents modulate the strength of intermolecular contacts is fairly well understood. For example, an electron-withdrawing group will typically pull electron density away from the interacting atom, deepening its σ or π -hole, and thereby strengthening the electrostatic attraction with a base. The situation becomes more complicated for an internal noncovalent bond where a substituent will influence the properties of both the acid and base atom, perhaps in different ways. For example, Sunoj and coworkers showed that an intramolecular chalcogen bond is regulated by the substituent at the *ortho* site of arylselenides.²⁶ Scheiner et al. observed that the strength of an intramolecular chalcogen bond is increased when an electron-withdrawing substituent is added to the site *ortho* to the ether and *meta* to SF₃ in phenyl-SF₃ molecules.²⁷ When an electron-withdrawing group (-F, -Cl, -Br, -CN, and -NC) replaces the H of the Lewis acid in 8-phosphinonaphthalen-1-amine, the intramolecular pnictogen bond is enhanced.²⁸ Buemi et al. have carried out systematic DFT studies of malonaldehyde derivatives and confirmed that substituents make significant contributions to the strength of its intramolecular H-bond.^{29,30}

As an intriguing addition to this conversation, Gilli et al.^{31,32} introduced the concept of intramolecular resonance-assisted hydrogen bonds (RAHBs) that are stronger than conventional HBs. The authors attributed the extra stability to π electron delocalization in the so-called quasi-ring. These ideas motivated numerous computational^{33,34} and experimental studies^{35,36} which

have not yet reached a consensus. Mo et al³⁷ presented an alternate view that the enhanced HB arises from the flow of charge from the HB donor to the acceptor through π -conjugation. Recently, Grosch et al.,³⁸ concluded that π polarization and σ charge transfer are the responsible factors. They emphasized that there is no resonance assistance in the sense of the interaction between σ charge transfer and π polarization. It has been demonstrated that the presence and formation of RAHBs have a prominent effect on the structures, stability, and spectral properties of relevant molecules.³⁹⁻⁴¹ For instance, RAHBs in mono- and dicarbaldehydes of 2,6-dihydroxynaphthalene result in a significant red shift of the absorption maxima of $\pi\pi^*$ transitions.³⁹ Regardless of the ultimate explanation, resonance-assisted stabilization has been observed in intramolecular beryllium bonds,⁴² magnesium bonds,⁴³ and halogen bonds.⁴⁴ Absent to this point, however, is a determination as to whether such enhancement is possible in triel bonds.

There is reason to suspect that these sorts of triel bonds might exist. Our survey of the Crystal Structure Database (CSD) noted several interesting candidates. Fig. 1 depicts three illustrative crystal structures that contain a putative resonance-enhanced triel bond (RATrB). The boron-containing fluorophore of π -extended *cis*-stilbene in BOBFEG⁴⁵ emits fluorescence with high quantum yield in the solid state. Since the bond length from B to O_{amide} is only 1.6 Å, even shorter than that to C_{sp2} (1.627 Å), there is the suggestion of a strong interaction between the B and O atoms. The high fluorescence quantum yield has been attributed to the rigid structure involving the B-containing five-membered ring. This molecule has a wide range of applications including molecular sensors and biological imaging. The crystal structure of PAFSIZ⁴⁶ displays a five-membered aluminacyclopropene planar ring. The distance of the Al \cdots O contact is 1.77 Å, shorter than the Al–C bond length of 1.989 Å. It is intriguing that both are shorter than the corresponding covalent radius sums (Al–O = 1.89 Å; Al–C = 2.01 Å).⁴⁷ The presence of the seven-membered aluminum nitrogen heterocycle seems to stabilize the five-membered ring involving Al. Systems such as these have received extensive attention because of applications in pharmaceuticals, agricultural chemistry, and materials science. HUFXUD⁴⁸ contains two five-membered rings, and the two In \cdots O distances are 2.334 Å and 2.330 Å. These distances are somewhat longer than the covalent radius sum (2.05 Å), suggesting strong In \cdots O noncovalent interactions. Inspired by the above X-ray crystal structures, a semi-rigid five-atom ring system is taken as a principal motif by which to explore the possibility of resonance-assisted intramolecular triel bonding.

The present study employs high-level quantum calculations to answer some of the pressing questions of this issue. In the first place, what is the bonding energy of a given TrB, and what is the effect of placing both acid and base group on the same molecule to form an intramolecular TrB. Can this bond be strengthened further by adding a certain degree of resonance to the system in which it occurs? The work is also interested in finding the effects of substituents. Would an electron-withdrawing substituent, for example, act to strengthen or weaken the TrB given the fact that it will influence both acid and base components. It has become understood that the depth of a σ or π -hole on the acid atom has a direct bearing on the strength of its

interaction with a nucleophile. We seek to understand whether such a relation exists also within the confines of an internal TrB. Is there a certain degree of electron mobility within the π -system of the ring, and how does any such mobility translate into aspects of aromaticity?

2. Systems and Theoretical Methods

In order to address these questions, a series of systems were constructed containing an intramolecular TrB. A S atom was placed on one end of a chain of C atoms to act as an electron donor, and a TrH_2 group on the other end, where Tr refers to Al and its heavier analogues Ga and In. A nonconjugated $-\text{CHCH}_2\text{CH}_2-$ alkyl chain connected the two to form a five-membered ring completed by the $\text{Tr}\cdots\text{S}$ triel bond. Conjugation was then introduced by removing two H atoms from the chain which was transformed into $-\text{CHCH}=\text{CH}-$ with a formal $\text{C}=\text{C}$ double bond. Each of the three H atoms on this conjugated system was systematically replaced by either electron-withdrawing NO_2 or donating CH_3 . There were also calculations carried out for purposes of comparison with pairs of separate molecules, connected by an intermolecular triel bond.

Ab initio calculations were performed at the MP2/aug-cc-pVTZ level. For the fourth-row In atom, the aug-cc-pVTZ-PP basis set including a pseudopotential was applied to partially account for relativistic effects.⁴⁹ Geometries were fully optimized and the resulting structures verified to be minima by frequency calculations. Interaction energies between pairs of separate molecules in acyclic systems were assessed as the difference between the energy of the complex and that of the monomer pair with their geometries taken from the complex. Using the counterpoise method of Boys and Bernardi,⁵⁰ this quantity was corrected for basis set superposition error (BSSE). The strengths of internal interactions within cyclic systems were assessed by indirect methods as described below. All calculations were performed using Gaussian 09 software.⁵¹

The wave function analysis-surface analysis suite (WFA-SAS) program⁵² was used to analyze the molecular electrostatic potential (MEP) on the $0.001 \text{ e Bohr}^{-3}$ isosurface. Using QTAIM software,⁵³ atoms in molecules (AIM) analysis was performed to obtain topological parameters of each bond critical point (BCP). Nuclear Independent Chemical Shift (NICS) was used to explore the level of aromaticity in the ring systems. The gauge-invariant atomic orbital GIAO method was used for chemical shielding tensor calculations. $\text{NICS}(1)_{zz}$ was evaluated as the chemical shielding at a point lying 1.0 \AA above the ring center, defined as the z direction of the heavy atom coordinates.^{54,55} A combination of NBO5.0⁵⁶ and Multiwfn⁵⁷ programs can provide information for normalized multicenter bond order, which is also used to estimate the aromaticity.⁵⁸

3. Results

The systems examined here are illustrated in Fig. 2. The structure in Fig. 2a contains an alkyl CHCH_2CH_2 group spanning the S and triel atoms so there are no π -bonds which can conjugate with $\text{C}=\text{S}$. By removing H atoms from C_1 and C_2 , a formal double $\text{C}=\text{C}$ bond is introduced into Fig. 2b which can conjugate with $\text{C}=\text{S}$, and adds the possibility of resonance enhancement to the internal $\text{Tr}\cdots\text{S}$ triel bond. R_1 , R_2 , and R_3 represent sites where the H atoms can be replaced by a substituent, in this case either NO_2 or CH_3 , in various combinations. The

corresponding analogues of O or B are also compared, and these systems are not considered here due to their larger interaction energies (Table S1).

Triel Bond Lengths

A primary measure of the strength of an intramolecular interaction is the distance between the two atoms involved. As a point of reference, the sum of vdW radii of the Al \cdots S, Ga \cdots S, and In \cdots S pairs are 3.74, 3.85, and 4.03 Å, respectively. Each of the R(Tr \cdots S) distances for the alkyl ring is considerably shorter than this reference value by more than 1 Å, suggesting there is an attractive force present. The normalized distance, representing the ratio of R(Tr \cdots S) to the vdW sum, is some 65-67%. Removing two of the H atoms to change the connecting group to -CH-CH-CH-, denoted H,H,H, with its possible resonance involvement, reduces the R(Tr \cdots S) distance by between 0.055 Å and 0.074 Å, suggesting an enhancement in the attractive force.

The following rows contain the R(Tr \cdots S) distances when one or more H atoms of the conjugated H,H,H system are replaced by the electron-withdrawing NO₂ or releasing CH₃ substituents. The next three rows of Table 1 show that the presence of NO₂ elongates the TrB suggestive of a certain degree of TrB weakening. As is evident in the last three columns, the stretching is somewhat more prominent when NO₂ adopts the R₃ position, closest to the S atom. The elongation tends to be more noticeable for the largest Tr atom, so is maximal at 0.058 Å for the R₃ position when Tr=In. Unlike the nitro group, the methyl substituent shortens the TrB, although the magnitude of this contraction is a bit smaller than the stretching occurring for NO₂. This effect is weakest for the central R₂ position and for Tr=Ga. When both substituents are present at the same time, the next six rows of Table 1 indicate no clear pattern. For example, if a NO₂ group occupies position 1, the TrB length decreases if Me is in position 2 but elongates if CH₃ is moved to position 3.

Triel Bond Energy

Evaluation of the strength of an intramolecular bond, triel or otherwise, is a thorny issue. The strength of an intermolecular bond is typically evaluated as the energy required to pull the two separate molecules apart, the so-called binding or interaction energy. To do so in an intramolecular setting is not possible without breaking covalent bonds within the system as a whole. The AIM view of bonding is helpful in this regard, as the properties of the bond critical point are commonly regarded as closely related to the bond strength, and there have been numerous studies that verified this relationship within the context of intermolecular bonds.⁵⁹⁻⁶¹ It is therefore logical to deduce that certain bond critical point properties ought to be similarly capable of providing an estimate of the strength of an intramolecular triel bond.

The electron density at the bond critical point ρ scales roughly with the bond strength as does the potential energy density at the same point V .^{62, 63} These quantities are compiled in Table 2 and show the expected bond strengthening on going from the first to the second row as the ring system becomes conjugated. The density increases by some 17-20%, and V rises in magnitude by about 25%, both signaling a stronger bond. When the NO₂ substituent is added, both of these

quantities drop in magnitude, consistent with the bond stretches noted in Table 1. On a percentage basis ρ lowers by some 3-12%, with the largest drops associated with In, and the R_2 position least susceptible to such change. The pattern is quite similar for the V quantities. The density rises when H is replaced by CH_3 , but by a smaller amount, less than 6%, and V becomes less negative by a similar percentage, again consistent with a small TrB strengthening. Also like the changes in TrB length, there is less predictability when both NO_2 and CH_3 substituents are added. For example, ρ rises for $R_1=\text{NO}_2$ and $R_2=\text{CH}_3$, but changes in the opposite direction when CH_3 is moved from R_2 to R_3 .

In addition to ρ and V , there are other properties of each bond critical point that are relevant to the strength of the bond. The Laplacian of the density is compiled in Table S2, along with the kinetic energy G , and the total energy density H . $\nabla^2\rho$ is positive in all cases, indicative of a noncovalent bond. As a kinetic energy parameter, all of the values of G are positive. The small negative values of H are suggestive that these triel bonds contain a certain degree of covalency.

One would like to translate some of these AIM parameters into a quantitative assessment of the bond energy. Previous work has demonstrated that V can offer a particularly good yardstick in this regard. Indeed, there have been previous calculations that extracted the intramolecular hydrogen bond⁶⁴ and tetrel bond energies,⁶⁵ from the potential energy density V . A crucial ingredient in applying this protocol is determining the specific relationship between V and the bond energy for a given set of systems. Since the latter can only be computed for an intermolecular bond between two separate entities, the systems of interest here were divided into two separate molecular entities. To accomplish this partition, the covalent bond between C_2 and C_3 was broken. A H atom was added to the dangling bond of each unit on the broken C_2 - C_3 bond. The $\text{SCR}_3\text{CR}_2\text{CR}_1\text{TrH}_2$ ring, for example, was divided into SCR_3H and $\text{HCR}_2\text{CR}_1\text{TrH}_2$ where each underlined H refers to the H atom that was added to each segment. The geometry of the resulting pair of separate molecules was fully optimized and the interaction energy between them evaluated and corrected for basis set superposition. This energy is compiled in Table S3, along with other properties of each pair. E_{int} is rather large, even exceeding 20 kcal/mol, in some cases. It may be noted as well that the range of intermolecular $R(\text{Tr}\cdots\text{S})$ distances in these pairs is quite similar to the intramolecular distance listed in Table 1, arguing for the validity of the parallels between these two sorts of systems.

Of greatest interest here, the intermolecular interaction energies are closely related to the properties of the intermolecular bond critical point, also compiled in Table S3. In particular, the relation between E_{int} and the potential energy density V at the intermolecular $\text{Tr}\cdots\text{S}$ BCP is illustrated in Fig. S1, for each of the three Tr atoms. There is a clear linear relationship, with a correlation coefficient of 0.99, regardless of the identity of the Tr atom. Importantly, all three $\text{Tr}\cdots\text{S}$ trend lines have a nearly identical slope of 0.48, regardless of the nature of Tr. The interaction energy can therefore be very closely approximated by the simple relationship of $E_{\text{int}}=0.48 V$. It is notable that an almost identical relationship of $E_{\text{int}}=0.5 V$ has been deduced for intramolecular H-bonds.⁶⁴

With this equation in hand, it was then possible to estimate the intramolecular triel bond

energies of the ring systems, based on their calculated V . These TrB energies are displayed in Table 3 and suggest that these bonds are rather strong, some exceeding 20 kcal/mol. Consistent with the triel bond lengths and AIM parameters, Ga engages in the strongest TrBs. The presence of the electron-withdrawing NO_2 group weakens the bond, while Me has the opposite effect, although these substituent effects are not very large. The resonance enhancement induced by the presence of the double bond within the C skeleton enhances the TrB strength by 3-4 kcal/mol, an enhancement by some 22-26%. These relationships are more clearly visible in Fig. 3 which plots the triel bond energy against the optimized $R(\text{Tr}\cdots\text{S})$ distance. Also linearly related to the TrB length are the bond critical point density and the potential energy density, illustrated in Figs. 4a and 4b, respectively. It is noted that the relationship between the binding distance and the electron density becomes exponential if the range is larger.⁶⁶⁻⁶⁸

Despite their different molecular structures, it is interesting to compare the TrB energies of the conjugated ring systems with the intermolecular systems formulated to resemble them to some degree. While the intramolecular bonds have the advantage of possible resonance enhancement, the separate molecules are free of the geometrical restrictions imposed by an intramolecular contact. These two factors are in balance with one another to some degree. As presented in Table S4, the intermolecular systems are bound more strongly for the $\text{Tr}=\text{Al}$ systems by some 3-6 kcal/mol. It is the conjugated intramolecular TrBs which are stronger, at least in most cases, for $\text{Tr}=\text{Ga}$. The two competing factors strike more of a balance for $\text{Tr}=\text{In}$ where the differences are smaller and of varying sign.

Energies Derived from Bond Rotations and π -Hole Depths

An alternate means of estimating the strength of an intramolecular interaction such as the triel bond considered here is breaking this bond by an internal rotation, but leaving the remainder of the system intact. Fig. 5a illustrates the optimized bond lengths contained within the alkyl unconjugated $\text{SCHCH}_2\text{CH}_2\text{AlH}_2$ system, which contrasts with the conjugated $\text{H,H,H SCHCHCHAlH}_2$ in Fig. 5b. A 180° rotation around the $\text{C}_1\text{-C}_2$ bond rotates the TrH_2 group of H,H,H away from S, replacing it by the H atom bound to the same C_1 , as pictured in Fig. 5c. Following this rotation, a full optimization of the trans geometry raised the energy of the H,H,H conjugated SCHCHCHAlH_2 system by 20.35 kcal/mol. Of course, this rotation does more than simply break the $\text{Al}\cdots\text{S}$ triel bond; it is also subject to other factors such as a possible $\text{H}\cdots\text{H}$ repulsion between the AlH_2 and the C_2H atom, and a redistribution of electron density throughout the entire system. Nonetheless, this energy rise is somewhat larger than the 14.4 kcal/mol extracted via the aforementioned BCP density protocol, so confirms that the values in Table 3 are likely not overestimates of the internal TrB energies.

A second independent measure of the TrB strength can be realized by a substitution. The replacement of the CHS group of CHSCHCHAlH_2 by CH_3 deletes the possibility of an internal TrB, as indicated in Fig. 5d. The configuration in which the AlH_2 group lies trans to CH_3 in Fig. 5e is calculated to be 1.55 kcal/mol more stable than the cis structure in Fig. 5d. So it is the internal TrB that is only possible for the full ring CHSCHCHAlH_2 that leads to the 20.35

kcal/mol preference for the cis configuration, another indication that the TrB strengths listed in Table 4 represent a reasonable estimate.

In the spirit of forces that contribute to the strength of noncovalent bonds, there is usually a high proportion of electrostatic attraction. The ability of the Tr atom to attract the negative region of the S ought to be related to the depth of the positive π -hole that lies above the Tr. Examples of the disposition of the MEP around the cyclic systems provided in Fig. S2 show this positive region near Tr, along with a negative region associated with the S. $V_{S,\max}$ was evaluated as the maximum in the MEP on the $\rho=0.001$ a.u. isodensity surface, and is displayed in Table 4. This quantity follows certain trends, one of which is that the hole is mildest for Ga, as compared to Al and In, which are roughly equal to one another. Comparison of the first two rows indicates the removal of the two H atoms which adds the conjugation to the ring intensifies the Tr π -hole by some 23-32%. Nitro substitution introduces a major increment, particularly in the C₂ position. The opposite effect of a diminished π -hole is caused by methyl substitution. The deepening influence of NO₂ is stronger than the lowering caused by methyl, and it is the former that dominates when both are present. It should be noted, however, that the π -hole depths listed in Table 4 occur in association with the TrB, so are not fully independent of this bond.

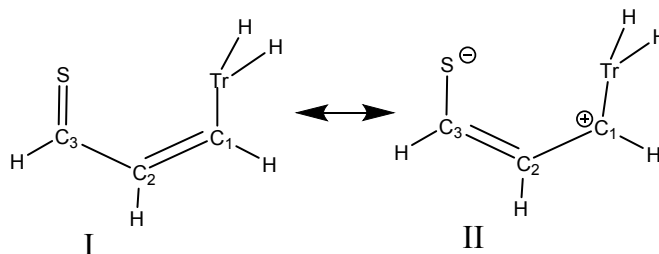
Bonding Pattern

An insightful perspective on the charge pattern surrounding each molecule can be gleaned by comparison of natural charges assigned to each atom. These charges on the Tr and S atoms listed in Table S5 indicate a high positive charge on Tr, some in excess of +1 e, while that on S is more muted, slightly negative in most cases, less than -0.1 e. The charge on the C₁ atom, abutting Tr, is also negative, more so than is S. The charges of the unconjugated and conjugated rings in the first two rows of Table S5 are suggestive of a resonance view of the electronic structure which is pictured in Scheme I. The double C₃=S and C₁=C₂ bonds of structure I both take on single bond character in structure II, bracketing a double C₂=C₃ bond. The lack of a π -orbital on Tr that is perpendicular to the ring prevents this atom from participating in the conjugation.

The transition to a conjugated ring has only a minor effect on the charge of Tr, becoming only slightly more negative, by some 0.06 e. The S atom, in contrast, takes on a bit more negative charge with this quantity rising by nearly 0.1 e. The most dramatic change occurs on C₁, whose charge becomes much more positive upon conjugation, rising by 0.5 e. This charge pattern is consistent with the incorporation of a certain contribution of resonance structure II to the principal bonding diagram of I.

The bond lengths of the conjugated system add support for a contribution of diagram II to the electronic structure. (The following numerical values apply to the Tr=Al systems in Fig. 5, but the patterns are characteristic of Al and Ga as well.) The removal of the two H atoms in Fig. 5a from C₁ and C₂ which introduces a double bond between these two atoms in Fig. 5b of course shortens this bond, from 1.528 Å to 1.359 Å. But the latter length is somewhat longer than its value of 1.351 Å in Fig. 5d and 5e where the absence of the C=S double bond eliminates the

possibility of conjugation. The longer C₁-C₂ in the conjugated system is indicative of some contribution from structure II which contains only a single bond between these two atoms. Regarding the other bonds within the molecule, the removal of the two H atoms also shortens the adjacent C₂-C₃ bond, by 0.056 Å, suggestive of the partial double bond character arising from structure II. There is a simultaneous lengthening of the C₃-S bond by 0.016 Å, also consistent with a partial II contribution.



Scheme I. Resonance diagrams of conjugated system.

As for the specific contribution of the S...Al triel bond to resonance/conjugation, comparison of Figs. 5b and 5c is especially instructive. Upon removal of this internal noncovalent bond by bond rotation, the C=S bond shortens, C₂-C₃ grows longer, and C₁-C₂ contracts. All of these changes reflect a lesser contribution from structure II in Scheme I. This pattern is reinforced by the densities of the bond critical points. Upon removing the two H atoms that add a double bond to C₁-C₂, the C₂-C₃ bond acquires partial double bond character, in the sense that its BCP density rises from 0.278 a.u. to 0.304 a.u.. The C₃-S bond is weakened with its density dropping from 0.242 a.u. to 0.237 a.u.. So it would be justified to claim that the internal TrB fosters the influence of resonance within the system.

An interesting insight into the possibility of conjugation within this ring can be gained by comparison with the cis conformation of 1,3-butadiene, which clearly has a high level of conjugation within the C=C-C=C chain. The two highest occupied orbitals of butadiene, both of π symmetry, are exhibited in Fig. 6a and 6b. The similarity to the two highest occupied π -orbitals of the H,H,H conjugated system in Fig. 6c and 6d are indicative of the similarities of the two systems, buttressing the idea of conjugation in the latter system.

Another measure of conjugation arises in connection with the NICS protocol which computes the NMR chemical shift in the center of the ring, so reflects a certain amount of ring current. It has been found that best results are often achieved in evaluating the z-component of this property 1 Å above the ring center, commonly referred to as NICS(1)_{zz}, and a more negative value is an indication of greater aromaticity via its ring current.^[54,55,69-71] This index is reported in Table 5 for the various systems considered here. Note first the large jump on going from the first to the second row where the conjugation has been introduced. Ring current increases in the order Ga < Al < In, similar to the TrB energy in that Ga is the strongest of the three. The NO₂ group reduces the aromaticity as compared to the increase caused by the methyl substituent. To place these values in context, malondialdehyde contains a classic intramolecular OH...O H-bond within a

conjugated ring structure. The NICS value of this molecule⁷² is only -1.55 ppm, smaller than the 3-11 ppm range of the conjugated rings in Table 5.

To further confirm a certain level of aromaticity in these rings, the normalized multicenter bond order of $\text{Tr}\cdots\text{S}$ in the five-membered ring was evaluated, and the results are presented in Table S6. The value of this quantity ranges between 0.30 and 0.34. This amount is comparable to, but somewhat smaller than that in benzene (0.6).⁵⁸ So according to this metric, the five-membered rings considered here are at least partially aromatic although not quite to the same degree as in the classic aromatic molecule benzene.

4 Discussion

The triel bonds studied in this article are somewhat stronger than those examined in most previous works. For example, the interaction energies calculated here range from 12 up to more than 20 kcal/mol. This uniquely stronger intramolecular TrB is ascribed to the unique resonance structure containing conjugated double bonds. The electron-withdrawing NO_2 group weakens the bond, while the donating CH_3 has the opposite effect. A series of systems containing intramolecular TrB are reported here, so it is interesting to compare with the case of intramolecular hydrogen, halogen, sulfur, and phosphorus bonds. For the intramolecular hydrogen bond in malondialdehyde derivatives, its bond energy ranges from 9.1 to 13.5 kcal/mol.^{73,74} For the five-membered closed ring system with an internal interaction between a halogen and chalcogen atom,⁴⁴ the possibility of conjugation with an internal double bond appears to boost the strength of the bond, and the effects of electron-withdrawing and releasing groups is similar to that observed here, but overall bond energies are a bit smaller. In $\text{CH}(\text{X})\text{-CH}_2\text{-CH}_2\text{YH}$ ($\text{X}, \text{Y} = \text{O}, \text{S}, \text{Se}$), the $\text{XH}\cdots\text{X}$ internal HB competes in strength with the $\text{X}\cdots\text{YH}$ chalcogen - chalcogen interaction,⁷⁵ the HB and the chalcogen -chalcogen interactions observed for saturated compounds are much weaker than those found for their unsaturated analogues. These interactions are enhanced through an increase of the charge delocalization within the system, in a mechanism rather similar to the so-called RAHB. A computational study of the intramolecular pnicoen bond in 1,8-bis-substituted aromatic naphthalene derivatives (ZXH and ZX_2 with $\text{Z} = \text{P}, \text{As}$ and $\text{X} = \text{H}, \text{F}, \text{Cl},$ and Br),⁷⁶ indicated that the 1,8 derivatives are more stable than the monosubstituted ones for those cases with $\text{X-Z}\cdots\text{Z-X}$ and $\text{F-Z}\cdots\text{Z-H}$ alignments, although the interaction energy is less than 10 kcal/mol.

While intramolecular interactions are ubiquitous for H-bonds, studies of intramolecular TrBs are relatively rare. In naphthyl-bridged amino-borane derivatives, an intramolecular $\text{B}\cdots\text{N}$ interaction was revealed by NBO analysis.⁷⁷ If the B atom in this $\text{B}\cdots\text{N}$ interaction is paired with another nucleophile, it is weakened.⁷⁸ Experimental evidence for a similar intramolecular link within naphthalene skeletons was detected in the Cambridge Structural Database.⁷⁹ Some compounds involving an intramolecular TrB with possible resonance have been successfully synthesized using a diboron molecule.⁸⁰

Within the context of H-bonds, as the ring system becomes conjugated,^{81,82} resonance enhances the interaction by some 2-6 kcal/mol. Other evidence of this phenomenon arises in the electron density and potential energy density which grow by 18-23% and 29%, respectively. For

the intramolecular RAtRB reported in this work, the electron density increases by some 17-20% and potential energy density rises in magnitude by about 25%, both signaling a stronger bond. The degree to which resonance enhances the RAHB and RAtRB systems depends on the carbon chain substituents. At the same time, the potential energy density of RAHB and RAtRB systems has a certain degree of correlation with the binding distance. These hydrogen and triel bonds may be classified as systems where the π -electron delocalization enhances the strength of the interaction. A previous study⁷² reported the value of resonance NICS (1) for six-membered and five-membered rings. The values of closed ring systems containing an intramolecular H-bond are all greater than -13 ppm.

A study of the redistribution of σ and π charges related to intramolecular hydrogen bond formation of malondialdehyde and its saturated analog 3-hydroxypropionaldehyde showed that the π charge flow indeed conforms to the Lewis structure proposed by the RAHB model.³⁸ This typical rearrangement of charge is only present in the unsaturated system, and not in its saturated analogue. Resonance in the π electron system assists the intramolecular hydrogen bond by reducing the hydrogen bond distance, and by providing an additional stabilizing component to the net bonding energy. This is in line with the recent work by Jiang and co-workers.^{83,84} The π polarization and σ charge-transfer interactions enhance the intramolecular hydrogen bond in malondialdehyde independently from each other. However, in the RAtRB system, the double $C_3=S$ and $C_1=C_2$ bonds of structure I both take on single bond character in structure II, bracketing a double $C_2=C_3$ bond. The lack of a π -orbital on Tr that is perpendicular to the ring prevents this atom from participating in the conjugation so the transition to a conjugated ring has only a minor effect on the charge of Tr. The most dramatic change occurs on C_1 , whose charge becomes much more positive upon conjugation. This indicates that the enhanced TrB is generated due to the flow of charges from the TrB donor to the acceptor through the π -conjugation, which is consistent with the view proposed by Mo et al.

5 Conclusions

The internal $Tr\cdots S$ triel bond within the five-membered ring is rather strong, between 12 and 21 kcal/mol. There is a certain degree of enhancement, 3-4 kcal/mol, associated with the resonance that arises from conjugation of a $C=C$ with the $C=S$ bond. This addition represents an increment of roughly 25%. Ga is associated with the strongest bonds in comparison with the smaller Al and larger In atoms. Adding electron-withdrawing NO_2 substituents to the ring tends to weaken the TrB, whereas an electron-donating methyl group has a strengthening effect. The analyses of MOs, NICS(1)zz and multicenter bond order show that the five-membered ring with an internal $Tr\cdots S$ triel bond has aromaticity to some of degree.

Conflicts of interest

There are no conflicts to declare.

Acknowledgements

This work was supported by the Natural Science Foundation of Shandong Province (ZR2021MB123), the US National Science Foundation (1954310), and the Yantai University Innovation Foundation (YDZD2111).

References

1. D. J. McClements, *Biotechnol. Adv.*, 2006, **24**, 621-625.
2. F. Q. Shi, X. Li, Y. Xia, L. Zhang and Z. X. Yu, *J. Am. Chem. Soc.*, 2007, **129**, 15503-15512.
3. A. Priimagi, G. Cavallo, P. Metrangolo and G. Resnati, *Acc. Chem. Res.*, 2013, **46**, 2686-2695.
4. S. Varughese, *J. Mater. Chem. C*, 2014, **2**, 3499-3516.
5. S. Scheiner, Hydrogen bonding: A theoretical perspective, *Oxford University Press*, New York, 1997.
6. M. M. Montero-Campillo, P. Sanz, O. M \acute{o} , M. Y \acute{a} ñez, I. Alkorta and J. Elguero, *Phys. Chem. Chem. Phys.*, 2018, **20**, 2413-2420.
7. A. Frontera and A. Bauz \acute{a} , *Chem. Eur. J.*, 2018, **24**, 7228-7234.
8. A. Bauz \acute{a} , I. Alkorta, J. Elguero, T. J. Mooibroek and A. Frontera, *Angew. Chem. Int. Ed.*, 2020, **132**, 17635-17640.
9. S. Zahn, R. Frank, E. Hey-Hawkins and B. Kirchner, *Chem. Eur. J.*, 2011, **17**, 6034-6038.
10. W. Wang, B. Ji and Y. Zhang, *J. Phys. Chem. A*, 2009, **113**, 8132-8135.
11. P. Metrangolo, H. Neukirch, T. Pilati and G. Resnati, *Acc. Chem. Res.*, 2005, **38**, 386-395.
12. A. Bauz \acute{a} and A. Frontera, *Angew. Chem. Int. Ed.*, 2015, **54**, 7340-7343.
13. A. Bauz \acute{a} , T. J. Mooibroek and A. Frontera, *Angew. Chem. Int. Ed.*, 2013, **52**, 12317-12321.
14. S. J. Grabowski, *ChemPhysChem*, 2014, **15**, 2985-2993.
15. R. Bonaccorsi, E. Scrocco and J. Tomasi, *J. Chem. Phys.*, 1970, **52**, 5270-5284.
16. S. J. Grabowski, *ChemPhysChem*, 2015, **16**, 1470-1479.
17. A. Bauz \acute{a} , X. Garc \acute{a} a-Llin \acute{a} s and A. Frontera, *Chem. Phys. Lett.*, 2016, **666**, 73-78.
18. D. Fiacco and K. Leopold, *J. Phys. Chem. A*, 2003, **107**, 2808-2814.
19. D. W. Bolen and G. D. Rose, *Annu. Rev. Biochem.*, 2008, **77**, 339-362.
20. Y. Zhou, G. Deng, Y. Z. Zheng, J. Xu, H. Ashraf and Z. W. Yu, *Sci. Rep.*, 2016, **6**, 1-8.
21. H. T. Huynh, O. Jeannin and M. Fourmigu \acute{e} , *Chem. Comm.*, 2017, **53**, 8467-8469.
22. H. Wang, J. Liu and W. Wang, *Phys. Chem. Chem. Phys.*, 2018, **20**, 5227-5234.
23. A. Franconetti, A. Frontera and T. J. Mooibroek, *CrystEngComm*, 2019, **21**, 5410-5417.
24. S. P. Gnanasekar and E. Arunan, *J. Phys. Chem. A*, 2018, **123**, 1168-1176.
25. A. Trujillo, I. Rozas, J. Elguero, I. Alkorta and G. S \acute{a} nchez-Sanz, *Phys. Chem. Chem. Phys.*, 2019, **21**, 23645-23650.
26. A. Roy and R. B. Sunoj, *J. Phys. Chem. A*, 2006, **110**, 5942-5947.
27. V. D. P. N. Nziko and S. Scheiner, *J. Org. Chem.*, 2015, **80**, 2356-2363.

28. G. Sanchez-Sanz, C. Trujillo, I. Alkorta and J. Elguero, *Phys. Chem. Chem. Phys.*, 2016, **18**, 9148-9160.
29. G. Buemi, *Chem. Phys.*, 2002, **277**, 241-256.
30. G. Buemi and F. Zuccarello, *Chem. Phys.*, 2004, **306**, 115-129.
31. G. Gilli, F. Bellucci, V. Ferretti and V. Bertolasi, *J. Am. Chem. Soc.*, 1989, **111**, 1023-1028.
32. P. Gilli, V. Bertolasi, L. Pretto, V. Ferretti and G. Gilli, *J. Am. Chem. Soc.*, 2004, **126**, 3845-3855.
33. R. W. Góra, M. Maj and S. J. Grabowski, *Phys. Chem. Chem. Phys.*, 2013, **15**, 2514-2522.
34. L. Sobczyk, S. J. Grabowski and T. M. Krygowski, *Chem. Rev.*, 2005, **105**, 3513-3560.
35. H. Houjou, T. Motoyama, S. Banno, I. Yoshikawa and K. Araki, *J. Org. Chem.*, 2009, **74**, 520-529.
36. K. T. Mahmudov and A. J. L. Pombeiro, *Chem. Eur. J.*, 2016, **22**, 16356-16398.
37. P. Sanz, O. Mó, M. Yáñez and J. Elguero, *ChemPhysChem*, 2007, **8**, 1950-1958.
38. A. A. Grosch, S. C. C. van der Lubbe and C. F. Guerra, *J. Phys. Chem. A*, 2018, **122**, 1813-1820.
39. H. Houjou, T. Motoyama, S. Banno, I. Yoshikawa and K. Araki, *J. Org. Chem.*, 2009, **74**, 520-529.
40. A. Gutiérrez-Quintanilla, M. Chevalier, R. Platakyte, J. Ceponkus, G. A. Rojas-Lorenzo and C. Crépin, *Phys. Chem. Chem. Phys.*, 2018, **20**, 12888-12897.
41. N. Wachter-Jurcsak and C. A. Detmer, *Org. Lett.*, 1999, **1**, 795-798.
42. M. M. Montero-Campillo, I. Alkorta, J. Elguero and M. Yáñez, *Molecules*, 2021, **26**, 3401.
43. P. Sanz, M. M. Montero-Campillo, O. Mó, M. Yáñez, I. Alkorta and J. Elguero, *Theor. Chem. Acc.*, 2018, **13**, 1-12.
44. A. V. Pandiyan, P. Deepa and P. Kolandaivel, *Phys. Chem. Chem. Phys.*, 2015, **17**, 27496-27508.
45. M. Nogami, K. Hirano, K. Morimoto, M. Tanioka, K. Miyamoto, A. Muranaka and M. Uchiyama, *Org. Lett.*, 2019, **21**, 3392-3395.
46. H. Zhu, J. Chai, Q. Ma, V. Jancik, H. W. Roesky, H. Fan and R. Herbst-Irmer, *J. Am. Chem. Soc.*, 2004, **126**, 10194-10195.
47. P. Pykkö and M. Atsumi, *Chem. Eur. J.*, 2009, **15**, 186-197.
48. Y. C. Park, CSD Communication (Private Communication). CCDC, Cambridge, England. 2015.
49. K. L. Schuchardt, B. T. Didier, T. Elsethagen, L. Sun, V. Gurumoorthi, J. Chase and T. L. Windus, *J. Chem. Inf. Model.*, 2007, **47**, 1045-1052.
50. S. F. Boys and F. Bernardi, *Mol. Phys.*, 1970, **19**, 553-566.
51. M. J. Frisch, G. W. Trucks, H. B. Schlegel, G. E. Scuseria, A. Robb, J. R. Cheeseman, G. Scalmani, V. Barone, B. Mennucci, G. A. Petersson, H. Nakatsuji, M. Caricato, X. Li, H. P. Hratchian, A. F. Izmaylov, J. Bloino, G. Zheng, J. L. Sonnenberg, M. Hada, M. Ehara, K. Toyota, R. Fukuda, J. Hasegawa, M. Ishida, T. Nakajima, Y. Honda, O. Kitao, H. Nakai, T.

- Vreven, J. Montgomery, J. E. Peralta, F. Ogliaro, M. Bearpark, J.J. Heyd, E. Brothers, K. N.Kudin, V. N. Staroverov, R. Kobayashi, J. Normand, K. Raghavachari, A. Rendell, J. C. Burant, S. S. Iyengar, J. Tomasi, M. Cossi, N. Rega, J. M. Millam, M. Klene, J. E. Knox, J. B. Cross, V. Bakken, C. Adamo, J. Jaramillo, R. Gomperts, R.E. Stratmann, O. Yazyev, A. J. Austin, R. Cammi, C. Pomelli, J. W. Ochterski, R. L. Martin, K. Morokuma, V. G. Zakrzewski, G. A. Voth, P. Salvador, J. J. Dannenberg, S. Dapprich, A. D. Daniels, O. Farkas, J. B. Foresman, J. V. Ortiz, J. Cioslowski and D. J. Fox, Gaussian 09, Revision D.01, Inc, Wallingford, CT 2009.
52. F. A. Bulat, A. Toro-Labbé, T. Brinck, J. S. Murray and P. Politzer, *J. Mol. Model.*, 2010, **16**, 1679-1691.
 53. T. A. Keith, AIMALL, version 13.05.06, TK Gristmill Software: Overland Park, KS, 2013.
 54. K. J. Donald, S. Gillespie and Z. Shafi, *Tetrahedron*, 2019, **75**, 335-345.
 55. R. Báez-Grez, D. Inostroza, V. García, A. Vásquez-Espinal, K. J. Donald and W. Tiznado, *Phys. Chem. Chem. Phys.*, 2020, **22**, 1826-1832.
 56. A. E. Reed, L. A. Curtiss and F. Weinhold, *Chem. Rev.*, 1988, **88**, 899-926.
 57. T. Lu and F. Chen, *J. Comput. Chem.*, 2012, **33**, 580-592.
 58. E. Matito, *Phys. Chem. Chem. Phys.*, 2016, **18**, 11839-11846.
 59. P. S. V. Kumar, V. Raghavendra and V. Subramanian, *J. Chem. Sci.*, 2016, **128**, 1527-1536.
 60. A. Filarowski and I. Majerz, *J. Phys. Chem. A*, 2008, **112**, 3119-3126.
 61. J. N. Woodford, *J. Phys. Chem. A*, 2007, **111**, 8519-8530.
 62. M. H. Abraham, R. J. Abraham, A. E. Aliev and C. F. Tormena, *Phys. Chem. Chem. Phys.*, 2015, **17**, 25151-25159.
 63. A. V. Afonin, A. V. Vashchenko and M. V. Sigalov, *Org & Biomol. Chem.*, 2016, **14**, 11199-11211.
 64. A. Espinosa, E. Molins and C. Lecomte, *Chem. Phys. Lett.*, 1998, **285**, 170-173.
 65. Y. X. Wei, Q. Z. Li, X. Yang and S. A. C. McDowell, *ChemistrySelect*, 2017, **2**, 11104-11112.
 66. J. E. Del Bene, I. Alkorta and J. Elguero, *Chem. Phys. Lett.*, 2017, **675**, 46-50.
 67. M. D. Esrafilii and R. Nurazar, *Mol. Phys.*, 2016, **114**, 276-282.
 68. M. Marín-Luna, I. Alkorta and J. Elguero, *Theor. Chem. Acc.*, 2017, **136**, 41.
 69. R. Báez-Grez, L. Ruiz, R. Pino-Rios, W. Tiznado, *RSC Adv.*, 2018, **8**, 13446-13453.
 70. J. J. Torres-Vega, A. Vásquez-Espinal, J. Caballero, M. L. Valenzuela, L. Alvarez-Thon, E. Osorio and W. Tiznado, *Inorg. Chem.*, 2014, **53**, 3579-3585.
 71. R. Báez-Grez, W. A. Rabanal-León, L. Alvarez-Thon, L. Ruiz, W. Tiznado and R. Pino-Rios, *J. Phys. Org. Chem.*, 2019, **32**, e3823.
 72. B. V. Pandiyan, P. Kolandaivel and P. Deepa, *Mol. Phys.*, 2014, **112**, 1609-1623.
 73. S. J. Grabowski, *J. Mol. Struct.*, 2001, **562**, 137-143.
 74. S. Wojtulewski and S. J. Grabowski, *J. Mol. Struct.-Theochem*, 2003, **621**, 285-291.
 75. P. Sanz, M. Yáñez and O. Mó, *Chem. Eur. J.*, 2003, **9**, 4548-4555.

76. D. Sánchez-Sanz, C. Trujillo, I. Alkorta and J. Elguero, *Phys. Chem. Chem. Phys.*, 2014, **16**, 15900-15909.
77. A. Pla, O. Sadek, S. Cadet, B. Mestre-Voegtlé and E. Gras, *Dalton Trans.*, 2015, **44**, 18340-18346.
78. W. Zierkiewicz, M. Michalczyk and S. Scheiner, *Molecules*, 2020, **25**, 635.
79. S. J. Grabowski, *Crystals*, 2019, **9**, 503.
80. A. Verma, R. F. Snead, Y. Dai, C. Slebodnick, Y. Yang, H. Yu and W. L. Santos, *Angew. Chem. Int. Ed.*, 2017, **129**, 5193-5197.
81. C. Fuster and S. J. Grabowski, *J. Phys. Chem. A*, 2011, **115**, 10078-10086.
82. A. Nowroozi, H. Hajiabadi and F. Akbari, *Struct. Chem.*, 2014, **25**, 251-258.
83. X. Jiang, H. Zhang, W. Wu and Y. Mo, *Chem. Eur. J.*, 2017, **23**, 16885-16891.
84. X. Lin, H. Zhang, X. Jiang, W. Wu and Y. Mo, *J. Phys. Chem. A*, 2017, **121**, 8535-8541.

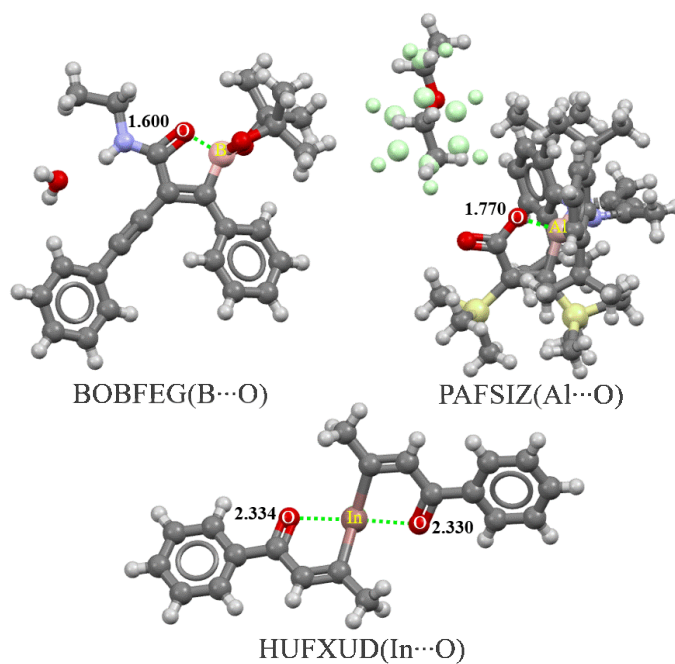


Fig. 1 Sample geometries extracted from the Cambridge Crystal Database (CSD) containing resonance-assisted intramolecular triel bond.

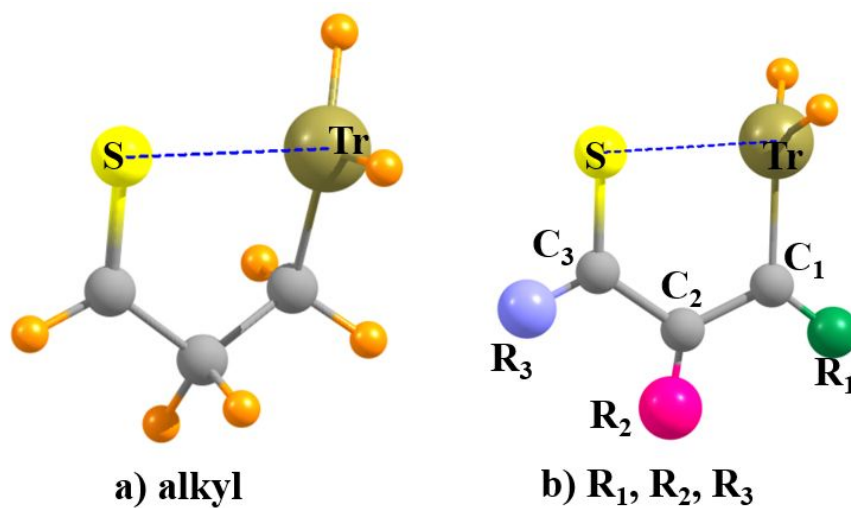


Fig. 2 Ring systems under study showing atomic labeling

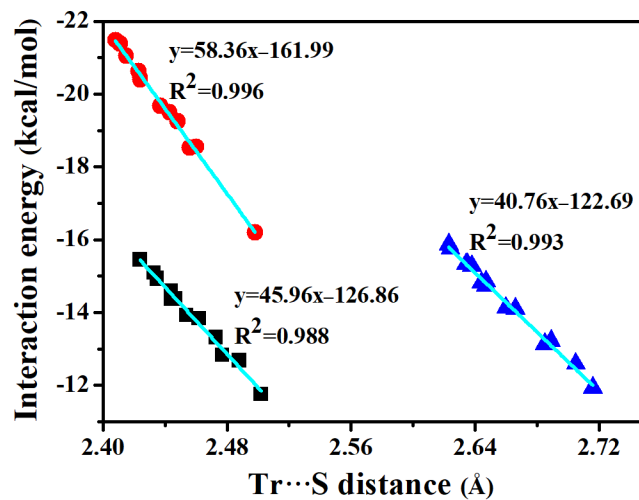


Fig. 3 Relationship between interaction energy and Tr...S distance. Symbols: black square, Al...S system; red circle, Ga...S system; blue triangle, In...S system.

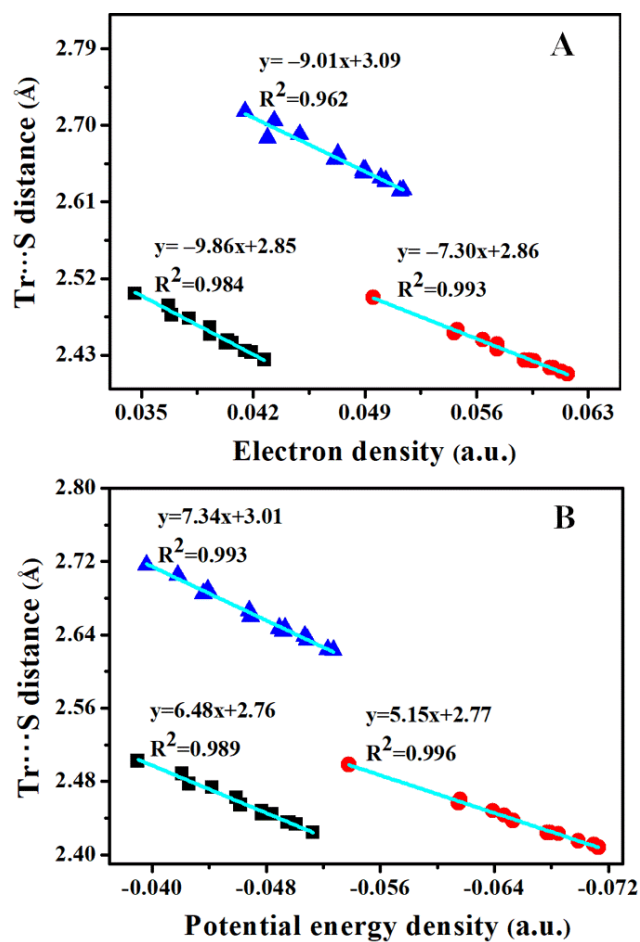


Fig. 4 The relationship of Tr...S distance with electron density (A) and potential energy density (B). Symbols: black square, Al...S system; red circle, Ga...S system; blue triangle, In...S system.

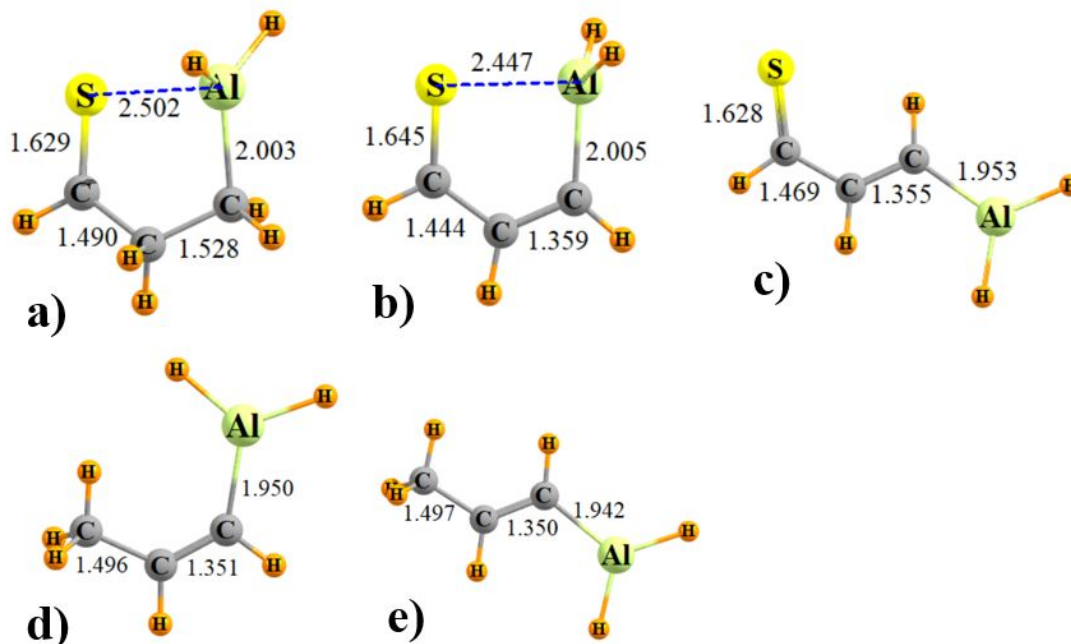


Fig. 5 Bond lengths (Å) in a) alkyl $\text{SCHCH}_2\text{CH}_2\text{AlH}_2$, and H,H,H conjugated SCHCHCHAlH_2 in its b) cis and c) trans configurations. The cis and trans geometries of $\text{CH}_3\text{CHCHAlH}_2$ are contained in d and e, respectively.

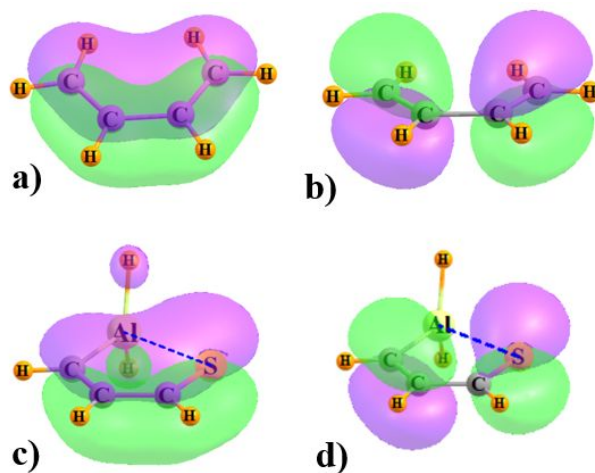


Fig. 6 a) HOMO-1 and b) HOMO molecular orbitals of cis-1,3-butadiene, in comparison with c) HOMO-4 and d) HOMO of the H,H,H $\text{Al}\cdots\text{S}$ conjugated system.

Table 1 Tr...S distance (Å) in ring systems^a and changes caused by substituents

R ₁	R ₂	R ₃	R(Tr...S)			ΔR(Tr...S) ^b		
			Al...S	Ga...S	In...S	Al...S	Ga...S	In...S
	alkyl		2.502	2.498	2.716			
H	H	H	2.447	2.424	2.647			
NO ₂	H	H	2.488	2.460	2.705	0.041	0.036	0.058
H	NO ₂	H	2.462	2.443	2.666	0.015	0.019	0.019
H	H	NO ₂	2.477	2.456	2.685	0.030	0.032	0.038
CH ₃	H	H	2.424	2.408	2.624	-0.023	-0.016	-0.023
H	CH ₃	H	2.444	2.424	2.644	-0.003	0.000	-0.003
H	H	CH ₃	2.435	2.415	2.634	-0.012	-0.009	-0.013
NO ₂	CH ₃	H	2.435	2.411	2.638	-0.012	-0.013	-0.009
NO ₂	H	CH ₃	2.473	2.448	2.689	0.026	0.024	0.042
CH ₃	NO ₂	H	2.433	2.415	2.635	-0.014	-0.009	-0.012
CH ₃	H	NO ₂	2.454	2.437	2.660	0.007	0.013	0.013
H	NO ₂	CH ₃	2.444	2.423	2.647	-0.003	-0.001	0.000
H	CH ₃	NO ₂	2.444	2.423	2.623	-0.003	-0.001	-0.024

^a Hu's van der Waals radii sum^[62] is equal to 3.74, 3.85, 4.03 Å respectively for Al...S, Ga...S, and In...S.

^brelative to H,H,H

Table 2 Electron density (ρ) and potential energy density (V) at the Tr...S BCP, all in a.u.

R ₁	R ₂	R ₃	ρ _{Al...S}	ρ _{Ga...S}	ρ _{In...S}	V _{Al...S}	V _{Ga...S}	V _{In...S}
	alkyl		0.0346	0.0495	0.0415	-0.0390	-0.0538	-0.0396
H	H	H	0.0404	0.0593	0.0489	-0.0477	-0.0679	-0.0489
NO ₂	H	H	0.0367	0.0548	0.0433	-0.0421	-0.0616	-0.0418
H	NO ₂	H	0.0393	0.0573	0.0473	-0.0459	-0.0647	-0.0468
H	H	NO ₂	0.0369	0.0546	0.0429	-0.0426	-0.0615	-0.0436
CH ₃	H	H	0.0427	0.0617	0.0514	-0.0513	-0.0713	-0.0523
H	CH ₃	H	0.0403	0.0590	0.0489	-0.0477	-0.0677	-0.0492
H	H	CH ₃	0.0415	0.0606	0.0503	-0.0495	-0.0699	-0.0509
NO ₂	CH ₃	H	0.0415	0.0613	0.0500	-0.0496	-0.0710	-0.0507
NO ₂	H	CH ₃	0.0380	0.0564	0.0449	-0.0442	-0.0639	-0.0439
CH ₃	NO ₂	H	0.0419	0.0608	0.0503	-0.0501	-0.0699	-0.0509
CH ₃	H	NO ₂	0.0393	0.0573	0.0471	-0.0462	-0.0653	-0.0469
H	NO ₂	CH ₃	0.0407	0.0596	0.0490	-0.0483	-0.0685	-0.0493
H	CH ₃	NO ₂	0.0407	0.0595	0.0512	-0.0484	-0.0685	-0.0527

Table 3 Intramolecular triel bond energy, $-E_{\text{int}}$ (kcal/mol)

			Al \cdots S	Ga \cdots S	In \cdots S
alkyl			11.75	16.20	11.93
H	H	H	14.37	20.45	14.73
NO ₂	H	H	12.68	18.55	12.59
H	NO ₂	H	13.83	19.49	14.10
H	H	NO ₂	12.83	18.52	13.13
CH ₃	H	H	15.45	21.48	15.75
H	CH ₃	H	14.37	20.39	14.82
H	H	CH ₃	14.91	21.05	15.33
NO ₂	CH ₃	H	14.94	21.39	15.27
NO ₂	H	CH ₃	13.31	19.25	13.22
CH ₃	NO ₂	H	15.09	21.05	15.33
CH ₃	H	NO ₂	13.92	19.67	14.13
H	NO ₂	CH ₃	14.55	20.63	14.85
H	CH ₃	NO ₂	14.58	20.63	15.87

Table 4 Maximum of electrostatic potential ($V_{S,\text{max}}$, kcal/mol) above Tr atom on $\rho=0.001$ a.u. isodensity surface

R ₁	R ₂	R ₃	Al \cdots S	Ga \cdots S	In \cdots S
alkyl			13.4	10.0	14.6
H	H	H	17.7	12.3	18.8
NO ₂	H	H	30.6	26.2	32.3
H	NO ₂	H	32.5	27.0	33.4
H	H	NO ₂	30.7	26.0	31.7
CH ₃	H	H	17.4	11.0	17.6
H	CH ₃	H	15.7	10.6	17.1
H	H	CH ₃	15.4	9.9	16.8
NO ₂	CH ₃	H	32.9	27.7	34.8
NO ₂	H	CH ₃	27.9	23.3	29.9
CH ₃	NO ₂	H	31.8	25.5	31.8
CH ₃	H	NO ₂	29.6	23.8	29.9
H	NO ₂	CH ₃	29.1	23.8	30.4
H	CH ₃	NO ₂	29.1	23.8	30.1

Table 5 NICS(1)_{zz} (ppm) 1 Å above center of the ring

R ₁	R ₂	R ₃	Al...S	Ga...S	In...S
	alkyl		-4.04	-3.66	-8.09
H	H	H	-7.98	-6.99	-10.43
NO ₂	H	H	-7.49	-6.52	-9.47
H	NO ₂	H	-7.61	-6.64	-9.58
H	H	NO ₂	-7.59	-6.60	-9.54
CH ₃	H	H	-10.90	-8.41	-11.16
H	CH ₃	H	-9.37	-7.88	-10.67
H	H	CH ₃	-9.98	-7.93	-10.95
NO ₂	CH ₃	H	-10.35	-8.33	-10.30
NO ₂	H	CH ₃	-7.60	-6.62	-9.55
CH ₃	NO ₂	H	-9.73	-7.58	-10.14
CH ₃	H	NO ₂	-7.79	-7.22	-9.58
H	NO ₂	CH ₃	-9.48	-7.90	-10.77
H	CH ₃	NO ₂	-9.48	-7.91	-10.84

